A simple, efficient polarizable coarse-grained water model for molecular dynamics simulations

Sereina Riniker and Wilfred F. van Gunsteren[a)]
Laboratory of Physical Chemistry, Swiss Federal Institute of Technology, ETH, 8093 Zürich, Switzerland

(Received 13 December 2010; accepted 20 January 2011; published online 28 February 2011)

The development of coarse-grained (CG) models that correctly represent the important features of compounds is essential to overcome the limitations in time scale and system size currently encountered in atomistic molecular dynamics simulations. Most approaches reported in the literature model one or several molecules into a single uncharged CG bead. For water, this implicit treatment of the electrostatic interactions, however, fails to mimic important properties, e.g., the dielectric screening. Therefore, a coarse-grained model for water is proposed which treats the electrostatic interactions between clusters of water molecules explicitly. Five water molecules are embedded in a spherical CG bead consisting of two oppositely charged particles which represent a dipole. The bond connecting the two particles in a bead is unconstrained, which makes the model polarizable. Experimental and all-atom simulated data of liquid water at room temperature are used for parametrization of the model. The experimental density and the relative static dielectric permittivity were chosen as primary target properties. The model properties are compared with those obtained from experiment, from clusters of simple-point-charge water molecules of appropriate size in the liquid phase, and for other CG water models if available. The comparison shows that not all atomistic properties can be reproduced by a CG model, so properties of key importance have to be selected when coarse graining is applied. Yet, the CG model reproduces the key characteristics of liquid water while being computationally 1–2 orders of magnitude more efficient than standard fine-grained atomistic water models.
 [doi:10.1063/1.3553378]

I. INTRODUCTION

Molecular dynamics (MD) simulations are a powerful tool to provide insight into molecular processes involving peptides and proteins. The system size and the time scale of atomistic simulations are, however, limited to tens of nanometers and nanoseconds by computational cost. A possible remedy is coarse graining (CG) of "unimportant" degrees of freedom, in which a group of atoms is represented by a single bead or particle. This may considerably reduce the number of particle–particle interactions to be calculated. Moreover, the interaction function describing the forces between coarse-grained particles will be a smoother function of their distance than that for the forces between atoms because of the averaging over the latter degrees of freedom. These two factors allow for an increased efficiency of up to orders of magnitude of CG versus all-atom fine-grained (FG) simulations.

There exists no general procedure to select degrees of freedom for coarse graining, and to determine how many of them are to be coarse grained and in what way. The type of "unimportant" degrees of freedom, e.g., bond-length vibrations in molecules, depends on the molecular property of interest, and the number of "unimportant" degrees of freedom depends on the scale of the phenomenon to be studied. Therefore, CG models found in the literature range from mapping of whole molecules or even groups of molecules onto one bead, as used in simulations of colloids or membranes, to systems where only two or three atoms are treated as one bead. In the present study, we focus on "small scale" coarse graining of water as this is the most important solvent in biomolecular systems. The solvent–solvent interactions, in particular for water, account for the bulk of the computational cost of atomistic biomolecular simulations, but their details are of minor interest. Thus, simulating these interactions at a lower resolution is particularly interesting as a means of enhancing the efficiency of biomolecular simulations.

In the past two decades, a large number of simple CG models have been developed for liquid water.[1–10] These models differ in the number of atoms per bead, i.e., the resolution, ranging from one water molecule per bead[1–3,6–8,10] to three[4,9] or even four.[5] All 1-to-1 models (one bead represents one water molecule) have one interaction site, except the two-site model of Izvekov and Voth.[7] The 1-to-1 mapping has the advantage that a comparison with experimental data is in principle straightforward, although one has to accept that coarse graining involves *per se* a loss of information,[10–13] but the speed-up compared with much used all-atom models that involve three interaction sites is rather limited. Models involving three or four water molecules per bead make simulations much more efficient, but at the expense of an increased difficulty to reproduce the properties of the underlying atomistic model.[14]

All simple CG models mentioned above model water, in principle, as a kind of van der Waals liquid with one interaction site per bead, where the electrostatic interactions are incorporated into an effective pairwise potential energy which

a)Electronic mail: wfvgn@igc.phys.chem.ethz.ch.

is either Lennard-Jones like, a Morse function or numerically represented. As there is no general procedure to derive such an effective potential energy function or to determine how many degrees of freedom can be coarse grained, different approaches can be taken. The most commonly used ones are center-of-mass-based techniques such as reverse Monte Carlo,[15] iterative Boltzmann inversion,[16] or force matching (FM),[7] which derive numerically represented CG forces on the beads from the underlying atomic-scale positions of the atoms or forces on the atoms. This approach, however, fails when multiple water molecules are mapped onto one bead.[9,14] Hence for lower resolution models, other approaches have to be used in which an effective potential energy function is either derived utilizing a clustering algorithm,[14] or through fitting to structural data or to thermodynamic properties such as density, compressibility, surface tension, and solvation free energies.[5,9] Note again that by coarse graining less properties than at the atomic level can be faithfully represented simultaneously. Thus, a limited number of properties of key importance have to be chosen for calibration depending on the property or process of interest. In addition, the effective interaction function depends, independently of the chosen approach, on the thermodynamic state point, i.e., temperature and pressure, at which it was calibrated or derived. The energy and entropy of the coarse-grained degrees of freedom at the specific state point are incorporated into the effective potential energy function, which is therefore not only limited in its representativity, but also in its transferability.[11]

Modeling the electrostatic interactions implicitly by incorporating them into an effective pairwise potential energy function is a challenge that must be met, as these interactions are crucial for the properties of highly dielectric compounds such as water. The electrostatic effects can only poorly be mimicked by a deep Lennard-Jones function, which can even lead to freezing of liquid water at room temperature, as was found for the MARTINI model.[17] Recently, new CG models were therefore developed which treat the electrostatics explicitly.[18–20] Borgis *et al.*[18] reported a coarse-grained solvent model (PCGS) with a 3-to-1 mapping, where the CG particles carry induced dipoles at their centers which interact with the solute generated electric field but not with each other. The solvent–solvent interactions consist only of a short-ranged Lennard-Jones like repulsive and a Gaussian attractive part. Use of a Gaussian function is computationally somewhat inefficient because the calculation of the nonbonded interactions is the most expensive part of a simulation. In addition, the functional form, $\exp(-r^2)$, of a Gaussian energy function for attractive forces is a poor approximation of the r^{-6} van der Waals or r^{-1} Coulomb function that govern attractive forces. Two other models with a 4-to-1 mapping and utilizing a dipolar representation of electrostatic interactions were proposed by Wu *et al.*[19] (BMW model) and Marrink *et al.*[20] (polarizable MARTINI model). Both are three-site models consisting of a van der Waals center and two covalently connected interaction sites resembling a huge H_2O molecule. In the BMW model, all three particles are charged, thus forming a multipole. Their relative positions are fixed, i.e., it is a rigid model. It uses a soft Born–Mayer–Huggins function for the van der Waals interactions between the centers of the beads which makes the combination with fine-grained, all-atom molecular models difficult. In the polarizable MARTINI model on the other hand, the dipole is formed solely by two oppositely charged interaction sites rigidly connected to the central site, whereas the central site interacts only through a Lennard-Jones function with the centers of the other beads. The angle between the two bonds connecting the two charged interaction sites with the center is variable which makes this MARTINI model polarizable. A deficiency of this model is that it freezes above the experimental freezing point of water, just like the original purely Lennard-Jones MARTINI model,[5,17] and that it has a too low surface tension compared with the experiment.

Here, we present a simpler, more efficient polarizable CG water model for use in combination with the GROMOS force field.[21] Based on an analysis of the cluster properties of the all-atom FG simple-point-charge (SPC) model[22] for liquid water, it uses a five-to-one mapping. A CG bead consists of only two particles with opposite charges. Both features lead to a maximum increase in simulation efficiency while preserving the most important thermodynamic and dielectric properties of liquid water. The standard GROMOS (Ref. 23) Lennard-Jones 12-6 function is used to represent van der Waals interactions. This makes the model efficient and easy to implement and compatible with most FG molecular models. The model was parametrized against experimental data for the density, surface tension, and relative static dielectric permittivity of water in the liquid phase at room temperature and pressure. Its liquid phase properties are calculated and compared with those of the all-atom FG SPC and SPC/E (Ref. 24) water models, with those of the two other mentioned CG water models that treat electrostatic interactions explicitly, and with the experimental data. In addition, the liquid phase properties of the CG model are compared with those of an all-atom FG SPC simulation in which five water molecules are held together to represent one bead by distance restraining their oxygen atoms.

II. METHODS

A. All-atom and coarse-grained models

The all-atom fine-grained water model used for parametrization of and comparison to the CG model is the SPC model.[22] As a CG bead represents multiple water molecules, SPC clusters of different size, i.e., $n = 1$–5 water molecules per cluster, were studied. The grouping of n water molecules into a cluster in an unrestrained simulation is not trivial and is further complicated by the neighbors changing over time. Therefore, a clustering algorithm was applied where the $(n - 1)$ nearest neighbors of each water molecule were determined in each configuration and stored as a cluster. Afterwards, when looping over pairs of clusters for analysis, the overlapping clusters, i.e., those sharing one or more water molecules, were excluded from the calculation of interactions, distances, etc. This procedure allowed for good statistics and clusters of near ideal size. However, this clustering algorithm could not be used for the calculation of properties, where the time evolution of a cluster was required. For such properties, simulations were performed in which the n molecules of a cluster were held together by distance restraints. The

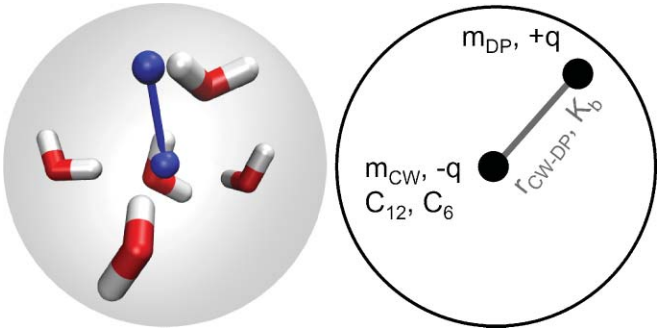

FIG. 1. Schematic representations of a bead of the CG water model representing five water molecules.

distances between the oxygen atom of the central water molecule of the cluster and the oxygens of the $(n-1)$ noncentral water molecules were restrained by an attractive half-harmonic potential energy function which was zero at a distance r_0 and became linear beyond a distance r_{lin}.[25]

The electrostatic interactions, which are dominating the potential energy between clusters, should be treated explicitly in the CG model. Thus, it consists of a spherical CG bead which has two electrostatic interaction sites, centre of water bead (CW) and dipole particle (DP), representing a polarizable dipole (Fig. 1). The first site, named CW, interacts with other CG beads through a pairwise Lennard-Jones and an electrostatic potential energy function, the former only applying to the CW sites and the latter to both the CW and the DP sites. The second interaction site is a so-called "dipole particle" which carries a charge opposite to that of the central site and interacts purely electrostatically, i.e., has no Lennard-Jones interaction, with the charged sites of other CG beads. The nonbonded potential energy between two sites i and j depends on their distance r_{ij} and has three contributions:

$$V_{\text{LJ}}^{ij}(r_{ij}) = \left(\frac{C_{12}(i,j)}{r_{ij}^6} - C_6(i,j)\right)\frac{1}{r_{ij}^6}, \tag{1}$$

$$V_c^{ij}(r_{ij}) = \frac{q_i q_j}{4\pi\epsilon_0\epsilon_{cs}}\frac{1}{r_{ij}}, \tag{2}$$

$$V_{rf}^{ij}(r_{ij}) = -\frac{q_i q_j}{4\pi\epsilon_0\epsilon_{cs}}\left(\frac{\frac{1}{2}C_{rf}r_{ij}^2}{R_{rf}^3} + \frac{1-\frac{1}{2}C_{rf}}{R_{rf}}\right), \tag{3}$$

where $R_{rf} = R_c$ is the cut-off and reaction-field radius, $C_{12}(i,j)$ and $C_6(i,j)$ the Lennard-Jones parameters, q_i the charge of particle i, and C_{rf} the Coulomb reaction-field constant which is defined as[23]

$$C_{rf} = \frac{(2\epsilon_{cs}-2\epsilon_{rf})(1+\kappa R_{rf}) - \epsilon_{rf}(\kappa R_{rf})^2}{(\epsilon_{cs}+2\epsilon_{rf})(1+\kappa R_{rf}) + \epsilon_{rf}(\kappa R_{rf})^2}. \tag{4}$$

The total nonbonded potential energy is obtained by summing over all ordered pairs (i,j) thereby taking into account the different nearest-neighbor and cut-off radius exclusions,[26]

$$\begin{aligned} V^{nb}(\vec{r}^N) = &\sum_{i=1}^{N-1}\sum_{\substack{j>i \\ j \text{ inside cut-off } i \\ (i,j) \text{ not excluded}}}^{N}\left(V_{LJ}^{ij}(r_{ij}) + V_c^{ij}(r_{ij})\right), \\ &+\sum_{i=1}^{N-1}\sum_{\substack{j>i \\ j \text{ inside cut-off } i}}^{N} V_{rf}^{ij}(r_{ij}), \\ &-\sum_{i=1}^{N}\frac{q_i^2}{4\pi\epsilon_0\epsilon_{cs}}\frac{1}{2}\left(\frac{1-\frac{1}{2}C_{rf}}{R_{rf}}\right), \end{aligned} \tag{5}$$

where the last term is a constant added to represent the self-interaction of the charged particles. For atomistic models, the dielectric permittivity inside the cut-off sphere $\epsilon_{cs} = 1$ whereas the CG model has $\epsilon_{cs} > 1$ which represents the dielectric response of the inside of a CG bead. The mass of the two particles, CW and DP, sums to the mass of five water molecules, whereas the ratio of the masses is an adjustable parameter of the model. The two interaction sites i and j of a bead that do not interact mutually through V_{LJ}^{ij} and V_c^{ij} are connected by an unconstrained bond with a half-attractive quartic potential energy function

$$V_{\text{bond}}^{\text{CG}}(r_{ij}) = \frac{1}{2}K_b(r_{ij} - r_{\text{CW-DP}})^4, \tag{6}$$

for $r_{ij} > r_{\text{CW-DP}}$, where $r_{\text{CW-DP}}$ sets a bound on the distance r_{ij} between particles i and j belonging to one CG bead. The use of a quartic instead of a harmonic attractive bond-length potential energy function makes the polarizability nonlinear[27] and has the advantage that overpolarization due to close distances between charges of different molecules is avoided as a result of the superlinear increase of the forces for longer bond lengths. The polarizability of the model resides in the free rotation of the DP particle around the central CW site and the oscillation of the bond connecting them, adjusting thus the dipole moment of a CG bead to the electric field of the environment.

B. Simulation details

All simulations were performed under isothermic-isobaric (NpT) conditions, if not stated otherwise, using a modified version of the GROMOS05 package of programs.[23] The temperature was kept at a reference value by weak coupling to a temperature bath with a coupling time of 0.1 ps,[28] and the pressure was maintained at 1.013 bar (1 atm) by the same type of algorithm using a coupling time of 0.5 ps. The integration time step was 2 fs. The energy, atom positions, and other relevant quantities were saved every 1.0 ps (500 steps) for analysis. For analysis of the FG SPC water properties available simulations at 303 K were used, whereas the CG model simulations were done at the slightly lower temperature of 298 K to ease comparison with experiment and literature.

TABLE I. Parameters for the half-harmonic attractive distance restraining between oxygen atoms of water molecules used in liquid phase simulations of SPC clusters. The ideal distance r_0, the distance r_{lin} beyond which the attractive half-harmonic energy function (Ref. 23) becomes linear, and the harmonic force constant K_d for clusters of n SPC water molecules, where n = 2–5, are given.

Cluster size, n	r_0 (nm)	r_{lin} (nm)	K_d (kJ mol^{-1} nm^{-2})
2	0.16	0.20	400
3	0.22	0.28	550
4	0.25	0.30	800
5	0.30	0.42	5000

1. Atomistic simulations

A cubic box with 12 800 SPC water molecules and an initial box length of 7.27 nm was used together with periodic boundary conditions. For the nonbonded interactions, a twin-range method was used with cut-off radii of 0.8 nm (short range) and 1.4 nm (long range). The force due to atoms beyond the long-range cut-off was modeled by a reaction-field force[29] representing a continuum with a relative dielectric permittivity ϵ_{rf} of 61.[30] The OH bond lengths and the H–H distance were constrained to the ideal SPC values with the SHAKE algorithm.[31] An isothermal compressibility of 4.575×10^{-4} (kJ mol^{-1} nm^{-3})$^{-1}$ was used in the pressure coupling. The pairlist for pairs within the short-range cut-off and the energies and forces for long-range pairs were updated every 10 fs (five time steps). After energy minimization, an equilibration simulation of 100 ps was carried out at 303 K. The SPC water box was then simulated for 3 ns, of which only the last 1.5 ns were used for analysis.

For the simulations with distance restraining between the oxygen atoms of SPC molecules of a cluster, the last configuration of the unrestrained simulation was used as starting configuration. In Table I, r_0, r_{lin} and the force constant K_d for the distance restraints are listed for the different cluster sizes n equal to 2–5. All systems were simulated for 2 ns at 303 K. For $n = 3$, only 12 798 SPC water molecules were used as 12 800 is not divisible by three.

For the simulation under canonical (NVT) conditions of a cluster of five water molecules *in vacuo*, stochastic dynamics was applied with a friction coefficient of 91 ps^{-1}. The temperature was raised from 100 to 303 K in steps of 50 K, each 1 ns long. At 303 K, the cluster was simulated for 10 ns.

The four different perturbations of the thermodynamic cycle performed with thermodynamic integration (TI) are shown in Fig. 2. The λ-dependence of the Hamiltonian is specified in Ref. 23. To avoid numerical instabilities as the nonbonded interactions between atoms are switched on or off during the perturbations a soft-core nonbonded interaction with $\alpha_{\text{LJ}} = 0.5$ and $\alpha_{crf} = 0.5$ nm^2 was used.[32] The simulations were carried out at 303 K under NVT conditions at 21 equally spaced λ-values between 0 and 1 with two additional λ-values between 0 and 0.1. For the three perturbations $\text{Cluster}_{\text{liquid}} \rightarrow \text{Cluster}_{\text{gas}}$, $\text{Cluster}_{\text{liquid}} \rightarrow \text{SPC}_{\text{liquid}}$, and $\text{SPC}_{\text{liquid}} \rightarrow \text{SPC}_{\text{gas}}$, two energy groups were defined: the first energy group consisted of molecules 1–5 forming a cluster and the second energy group of all other water molecules. For the perturbation $\text{Cluster}_{\text{liquid}} \rightarrow \text{Cluster}_{\text{gas}}$, the interactions between the two energy groups were scaled by a factor that decreased from 1.0 (liquid) to 0.0 (gas) at 23 λ-values, each simulated for 300 ps (after 150 ps equilibration). As starting configuration for all λ-values, the last configuration of the unperturbed distance restraining simulation was taken. For the perturbation $\text{Cluster}_{\text{liquid}} \rightarrow \text{SPC}_{\text{liquid}}$, the four noncentral water molecules in the cluster were perturbed to dummies, i.e., having zero nonbonded interactions, while leaving the distance restraints unchanged. As starting configuration for all λ-values, the last configuration of the unperturbed distance restraining simulation was taken. Simulations at each λ-value were 200 ps long after 100 ps equilibration. The configuration at $\lambda = 1$ (liquid) was used further for the perturbation $\text{SPC}_{\text{liquid}} \rightarrow \text{SPC}_{\text{gas}}$, where the central nondummy water molecule in the cluster was perturbed to dummy. Simulations at each λ-value were 400 ps long after 50 ps equilibration. For the perturbation $\text{Cluster}_{\text{gas}} \rightarrow \text{SPC}_{\text{gas}}$, stochastic dynamics (SD) simulations with a friction coefficient of 91 ps^{-1} were performed using the same perturbation procedure as for $\text{Cluster}_{\text{liquid}} \rightarrow \text{SPC}_{\text{liquid}}$. Simulations at each λ-value were 2 ns long after 100 ps equilibration.

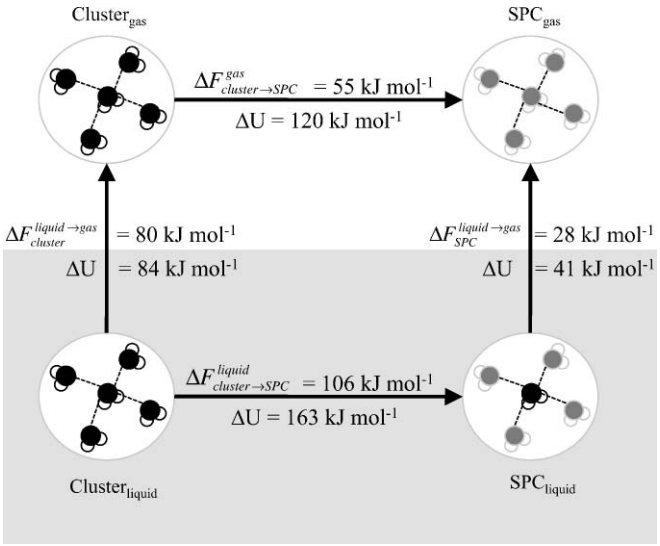

FIG. 2. Thermodynamic cycle between clusters of SPC water molecules and single SPC water molecules in the gas and in the liquid phase. Clusters are held together by distance restraints (black dashed lines).

2. Coarse-grained simulations

A cubic box with 2560 CG beads, i.e., 5120 particles, and an initial box length of 7.27 nm was used together with periodic boundary conditions. For the nonbonded interactions, a single-range cut-off radius of 2.0 nm was applied. For the interactions outside the cut-off, a reaction-field force[29] with a relative dielectric permittivity ϵ_{rf} of 78.5 was used.[33] The pairlist for pairs within the cut-off was updated every 10 fs (five time steps). For the electrostatic interactions within the cut-off sphere, a dielectric permittivity ϵ_{cs} of 2.5 was used. An isothermal compressibility of 7.51×10^{-4} (kJ mol^{-1} nm^{-3})$^{-1}$ was used in the pressure coupling. At 298 K, an equilibration of 100 ps with an integration time step of 2 fs was carried out and subsequently, a production run of 1 ns was performed, which was used for analysis. For the calculation of the thermal

expansion coefficient α and the heat capacity C_p, the system was additionally simulated for 1 ns, after 100 ps equilibration, at 318 and 338 K under NpT conditions. To observe the behavior of the system at lower temperatures, additional simulations at 278 and 258 K were carried out. For the calculation of the isothermal compressibility κ_T, NVT simulations of 1 ns length at three different densities $\rho = 0.947$, 0.997, and 1.047 g cm^{-3} were performed at 298 K. To derive the surface tension γ, five additional 1 ns NVT simulations with different starting velocities were carried out, where the box length in z-direction was extended to 35 nm. The shear viscosity η was calculated from a 1 ns NVT simulation where the elements of the pressure tensor were saved every 0.1 ps.

To obtain the excess free energy for the CG model, a TI simulation under NVT conditions was performed at 298 K, where all CG beads were perturbed to dummies along 21 equally spaced λ-values. The simulation at each λ-value was 100 ps long with 50 ps equilibration, and as starting configuration for all λ-values, the last configuration of the unperturbed simulation was used.

To check the influence of the size of the integration time step on the energy conservation, simulations under microcanonical (NVE) conditions were carried out at 298 K using different integration time steps $\Delta t = 2$, 5, 10, 15, 20, 25, and 28 fs, and a cut-off radius of 2.0 nm. The simulations were performed for 2000 steps, while the pairlist was updated every step and the energies were saved every step. Additional NVE simulations with an enlarged cut-off radius of 3.5 nm and integration time steps $\Delta t = 1$, 2, 5, 10, 15, 20, and 25 fs were carried out for 5000 steps at 298 K and the energy fluctuations were monitored.

C. Analysis

1. Intercluster and intracluster potential energy $V_{\text{pot}}^{\alpha\beta}(r)$ and $V_{\text{pot}}^{\alpha\alpha}$

The nonbonded potential energy $V_{\text{pot}}^{\alpha\beta}$ between two clusters α and β ($\alpha \neq \beta$) as a function of the intercluster distance $r_{\alpha\beta}$, i.e., the distance between the centers of geometry of the two clusters α and β was calculated using Eqs. (1)–(3)

$$V_{\text{pot}}^{\alpha\beta}(r_{\alpha\beta}) = \sum_{i=1}^{N_\alpha} \sum_{j=1}^{N_\beta} V_{LJ}^{ij}(r_{ij}) + V_c^{ij}(r_{ij}) + V_{rf}^{ij}(r_{ij}), \quad (7)$$

where N_α is the number of interaction sites in cluster α. Note that the clusters can penetrate each other resulting in shorter intercluster distances $r_{\alpha\beta}$ than can be found for the CG model. The intracluster nonbonded potential energy $V_{\text{pot}}^{\alpha\alpha}$ was calculated using the same Eqs. (1)–(3) and (7), but in this case the energy was simply summed up for each cluster.

2. Radial distribution function g(r)

The radial distribution function (RDF) $g(r)$ of the SPC water clusters was calculated using

$$g(r) = \frac{1}{4\pi(N-1)\rho r^2 \Delta r} \sum_{\alpha=1}^{N-1} \sum_{\beta>\alpha}^{N} \delta(r_{\alpha\beta} - r), \quad (8)$$

where N is the number of clusters, $r_{\alpha\beta}$ is the distance between the centers of geometry of two clusters α and β, and ρ is the density. The second part of the equation counts all clusters, that are at a distance r of each other.

3. Dipole moment, μ

The distribution of the dipole moment $\vec{\mu}$ of a cluster was calculated by summation of the product of the charges and the relative positions of the partial atomic charges in a cluster,

$$\vec{\mu} = \sum_{i=1}^{N_c} q_i \cdot (\vec{r}_i - \vec{r}_{\text{COG}}), \quad (9)$$

where N_c is the number of partial charges in a cluster, $\vec{r}_i$ is their positions, and $\vec{r}_{\text{COG}}$ is the position of the centre of geometry of the cluster.

To obtain the rotational correlation time τ_{rot} of the cluster dipole moment, the clusters were monitored over time and the autocorrelation function $C_{\text{rot}}(t)$ of $\vec{\mu}(t)$ was calculated using

$$C_{\text{rot}}(t) = \langle \vec{\mu}(\tau) \cdot \vec{\mu}(\tau + t) \rangle_{\tau,\text{clusters}} = A \ \exp\left(-\frac{t}{\tau_{\text{rot}}}\right). \quad (10)$$

$C_{\text{rot}}(t)$ shows in general an exponential decay, which thus can be fitted by the expression shown in Eq. (10), where A is a constant.

4. Self-diffusion coefficient, D

The diffusion coefficient D was obtained from the long-time limit of the mean-square displacement using the Einstein relation,[34]

$$D = \lim_{t\to\infty} \frac{\langle (\vec{r}(\tau + t) - \vec{r}(\tau))^2 \rangle_{\tau,\text{clusters}}}{6t}, \quad (11)$$

where $\vec{r}(t)$ is the position of the COG of a cluster at time t and the averaging was performed over both time and clusters. Equation (11) can be applied directly or through fitting of the linear regime of the time evolution.

5. Thermal expansion coefficient, α

The thermal expansion coefficient α of the CG model was obtained using the finite-difference expression,[35]

$$\alpha = \frac{1}{V}\left(\frac{\partial V}{\partial T}\right)_p \approx -\left(\frac{\ln\left(\frac{\rho_2}{\rho_1}\right)}{T_2 - T_1}\right)_p, \quad (12)$$

where V is the volume of the system, T the temperature, and ρ the density.

6. Heat capacity, C_p

The heat capacity at constant pressure can be approximated[36] using the relation

$$C_p \approx \frac{U_2^{\text{tot}} - U_1^{\text{tot}}}{T_2 - T_1} + \frac{\partial Q}{\partial T}, \quad (13)$$

where U^{tot} is the total energy per molecule or bead, and Q is the sum of the quantum contribution of the intramolecular

vibrational modes and the difference between the quantum mechanical and classical intermolecular vibrational energy. These quantum contributions add up to about –9.3 J mol^{-1} K^{-1} at 298 K and 1 atm.

7. Isothermal compressibility, κ_T

The isothermal compressibility κ_T of the CG model was calculated using the finite-difference expression,[37]

$$\kappa_T = -\frac{1}{V}\left(\frac{\partial V}{\partial p}\right)_T = \frac{1}{\rho}\left(\frac{\partial \rho}{\partial p}\right)_T = \left(\frac{\partial \ln(\rho)}{\partial p}\right)_T \approx \left(\frac{\ln\left(\frac{\rho_2}{\rho_1}\right)}{p_2 - p_1}\right)_T \tag{14}$$

8. Surface tension, γ

The surface tension γ of the CG model was obtained through time averaging over the diagonal elements p_{ii} of the pressure tensor using

$$\gamma = \frac{L_z}{2}\left\langle p_{zz} - \frac{1}{2}(p_{xx} + p_{yy})\right\rangle, \tag{15}$$

where L_z is the box length in the z-direction. The surface tension was further averaged over the five simulations with different starting velocities.

9. Shear viscosity, η

The shear viscosity was calculated using the Einstein relation

$$\eta = \frac{1}{2}\frac{V}{k_B T}\lim_{t\to\infty}\frac{d}{dt}\left\langle \Delta P_{\alpha\beta}^2(t)\right\rangle \quad \alpha\beta = xy, xz, yz, \tag{16}$$

where V is the volume of the box, T is the temperature, and $\Delta P_{\alpha\beta}(t)$ is the "displacement" of the off-diagonal elements of the pressure tensor $P_{\alpha\beta}(t)$ which is defined as follows:

$$\Delta P_{\alpha\beta}(t) = \int_0^t P_{\alpha\beta}(t')dt' \quad \alpha\beta = xy, xz, yz, \tag{17}$$

with

$$P_{\alpha\beta}(t) = \frac{1}{V}\left(\sum_{i=1}^{N}\frac{p_{\alpha i}(t)p_{\beta i}(t)}{m_i} + \sum_{i=1}^{N-1}\sum_{j>i}^{N} f_{\alpha ij}(t)r_{\beta ij}(t)\right), \tag{18}$$

where α and β are the x-, y-, or z-components, $p_{\alpha i}$ is the α-component of the momentum of particle i, $f_{\alpha ij}$ is the α-component of the force exerted on particle i by particle j, and $r_{\beta ij}$ is the β-component of the interparticle distance vector $\vec{r}_{ij} = \vec{r}_i - \vec{r}_j$. Because of poor statistics at long simulation times, the shear viscosity was calculated from the slope of $\Delta P_{\alpha\beta}^2(t)$ between 2 and 7 ps.

10. Relative static dielectric permittivity, $\epsilon(0)$

The relative static dielectric permittivity $\epsilon(0)$ was calculated by applying a constant homogeneous external electric field $\vec{E}^{\text{ext}}$ and measuring the response of the polarization $\vec{P}$,[26]

$$\epsilon(0) = 1 + 4\pi\frac{\langle P_z\rangle}{E_z^{\text{ext}}}, \tag{19}$$

where $\vec{P}$ can be calculated from the total dipole moment $\vec{M}$ of the system and its volume V,

$$\vec{P} = \frac{\vec{M}}{V} = \frac{1}{V}\sum_{i=1}^{N} q_i\vec{r}_i \tag{20}$$

For small field strengths, the response of $\vec{P}$ to $\vec{E}^{\text{ext}}$ is linear and can be fitted with linear regression.

D. Parametrization of the CG model

In the SPC cluster analysis, a cluster size of $n = 5$ was found to be optimal because of its spherical shape, which can be easily represented by a simple sphere at the coarse-grained level. The proposed model for CG water embedding five atomistic water molecules in a single bead with two interaction sites was parametrized to reproduce the experimental density and relative static dielectric permittivity of water at 298 K and 1 atm, while keeping the system in the liquid phase. The latter property was selected as it is of importance in characterizing the electrostatic effects of water. Using this approach, the following parameters were found. The charge of the CW particle is –0.575e and +0.575e for the DP particle. The mass of CW is 60.077 amu and of DP 30.0 amu, summing to the mass of five water molecules. The ratio of the masses was an adjustable parameter used to reproduce the rotational correlation time of the dipole moment of a SPC cluster of five water molecules in the liquid phase. The Lennard-Jones parameters of CW are $\epsilon_{\text{LJ}} = 1.5$ kJ mol^{-1} and $\sigma = 0.495$ nm which correspond to $C_6 = 0.088$ kJ mol^{-1} nm^6 and $C_{12} = 1.298\times10^{-3}$ kJ mol^{-1} nm^{12}. For the bond connecting the two particles in a bead, a force constant K_b of 2.0×10^6 kJ mol^{-1} nm^{-4} and an ideal distance $r_{\text{CW–DP}}$ of 0.2 nm were used. Due to the bigger volume of a CG bead compared with a SPC molecule, the cut-off radius for the nonbonded interaction beyond which interactions are approximated using a dielectric continuum reaction field had to be increased. A value of 2.0 nm was judged to be sufficient, as the error in the Lennard-Jones interaction became smaller than 1.5% at this distance. A dielectric permittivity $\epsilon_{cs} > 1$ inside the cut-off sphere was chosen to represent the dielectric response of the virtual internal degrees of freedom of a CG bead as a mean-field response. A value $\epsilon_{cs} = 2.5$ was found to give a relative static dielectric permittivity $\epsilon(0)$ of the model close to the experimental one.

E. Pressure correction for multiple-molecule CG bead models

In GROMOS, the hydrostatic pressure is defined using the virial theorem,

$$P(t) = \frac{2}{3}\frac{E_{\text{kin,mol}}(t) - W_{\text{mol}}(t)}{V(t)}, \tag{21}$$

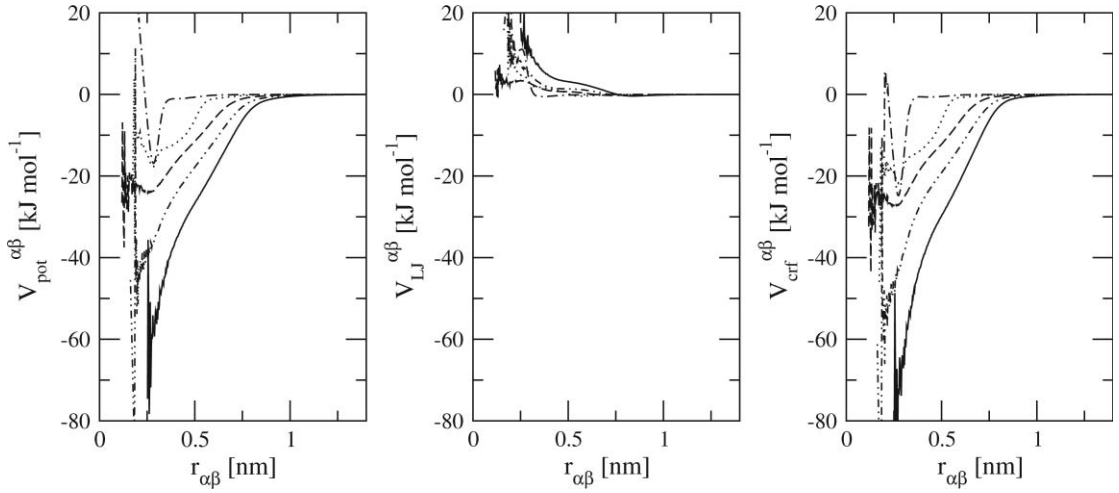

FIG. 3. The *inter*cluster nonbonded potential energy $V_{\text{pot}}^{\alpha\beta}$ [Eq. (7)] and its components $V_{\text{LJ}}^{\alpha\beta}$ and $V_{crf}^{\alpha\beta} = V_c^{\alpha\beta} + V_{rf}^{\alpha\beta}$ of SPC clusters averaged over all clusters (α, β) as a function of the *inter*cluster distance $r_{\alpha\beta}$ with $n = 1$ (dotted-dashed), 2 (dotted), 3 (dashed), 4 (double-dotted-dashed), or 5 (solid) water molecules in a simulation of liquid water at 303 K and 1 atm.

where $E_{\text{kin,mol}}(t)$ is the molecular translational kinetic energy, $W_{\text{mol}}(t)$ is the molecular virial, and $V(t)$ is the volume of the computational box. In the coarse-graining approach applied here, the kinetic energy and the virial pressure per molecule or bead are to be retained between the fine- and coarse-grained simulation. As a coarse-grained bead has five times less molecules than a corresponding cluster, $E_{\text{kin,mol}}(t)$ and $W_{\text{mol}}(t)$ are five times smaller compared with the fine-grained simulation. This reduction is corrected for by applying a coarse-graining factor

$$s_{\text{CG}}^{\text{tot}} = \frac{1}{N_a} \sum_{i=1}^{N_a} s_{\text{CG},i}, \tag{22}$$

to the right-hand side of Eq. (21), where N_a is the total number of atoms or particles, respectively, in the system. For a coarse-grained particle $s_{\text{CG}} = 5$, whereas for a fine-grained atom $s_{\text{CG}} = 1$.

III. RESULTS

A. All-atom SPC cluster analysis

1. Unrestrained simulations

Intercluster potential energy. The nonbonded potential energy $V_{\text{pot}}^{\alpha\beta}(r_{\alpha\beta})$ between clusters of n water molecules is shown in Fig. 3. The main contribution to the potential energy is the electrostatic interaction, and this electrostatic potential energy in turn is governed by the interaction between the closest water molecules. This can be seen by the fact that both $V_{crf}^{\alpha\beta} = V_c^{\alpha\beta} + V_{rf}^{\alpha\beta}$ for $n = 1$ at $r \simeq 0.25$ nm and $V_{crf}^{\alpha\beta}$ for $n = 5$ at $r \simeq 0.5$ nm (the intercluster distance corresponding to the correct density) are roughly –25 kJ mol^{-1}. Because in the CG model the entropy of the $n = 5$ FG water molecules is missing, a direct fitting of the potential energy of a CG liquid to this value leads to freezing of the CG liquid.

Intracluster potential energy. The nonbonded potential energy $V_{\text{pot}}^{\alpha\alpha}$ between the water molecules inside a cluster α was calculated and averaged for the liquid and for the gaseous phase. This energy is omitted when coarse graining is applied. In Table II, $V_{\text{pot}}^{\alpha\alpha}$ is shown for the different cluster sizes. In the liquid phase, the cluster energy decreases with n with an amount per added water molecule that monotonically decreases from 19.2 kJ mol^{-1} for $n = 2$–3 to 15 kJ mol^{-1} for $n = 4$–5. In the gas phase, the amount only starts to decrease for $n = 4$–5 and is much larger. This is due to the geometry of the water molecules, which allows for optimal hydrogen bonding of four molecules in the gas phase. Thus, the values for the liquid and the gaseous phase diverge increasingly with increasing cluster size.

Dipole moment distribution. The distribution of the dipole moment μ of a cluster was calculated for cluster sizes $n = 2$–5 and is shown in Fig. 4. The increase in the average dipole moment by adding additional water molecules to the

TABLE II. The *intra*cluster nonbonded potential energy of a cluster of $n = 2$–5 water molecules in the liquid phase (l) at 1 atm and *in vacuo* (g) at 303 K from MD simulation of SPC clusters. The potential energies V are defined in Eqs. (1)–(3) and (7), while $V_{crf} = V_c + V_{rf}$. The dipole moment μ is defined in Eq. (9). The diffusion coefficients D [Eq. (11)] were obtained for $n \geq 2$ from MD simulations in which clusters of water molecules were held together by restraining their oxygen–oxygen distances.

Cluster size, n	$V_{\text{pot}}^{\alpha\alpha}$(l) (kJ/mol)	$V_{\text{LJ}}^{\alpha\alpha}$(l) (kJ/mol)	$V_{crf}^{\alpha\alpha}$(l) (kJ/mol)	$V_{\text{pot}}^{\alpha\alpha}$(g) (kJ/mol)	$V_{\text{LJ}}^{\alpha\alpha}$(g) (kJ/mol)	$V_{crf}^{\alpha\alpha}$(g) (kJ/mol)	$\langle\mu\rangle$(l) (Debye)	$\langle\mu\rangle$(g) (Debye)	D(l) (cm^2 s^{-1})
2	–18.4	11.1	–29.5	–18.6	4.3	–22.9	3.7	4.9	2.3×10^{-5}
3	–37.6	16.7	–54.3	–48.3	11.5	–59.8	4.7	4.2	1.6×10^{-5}
4	–54.5	19.4	–73.8	–92.5	22.5	–115.0	5.5	2.9	1.2×10^{-5}
5	–69.5	20.8	–90.2	–119.9	28.6	–148.5	6.1	2.3	0.93×10^{-5}

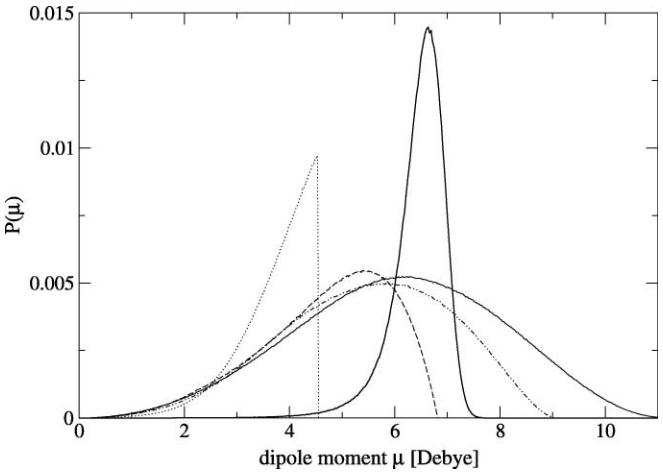

FIG. 4. The distribution of the cluster dipole moment μ [Eq. (9)] in liquid water for clusters with $n = 2$ (fine, dotted), 3 (fine, dashed), 4 (fine, double-dotted-dashed), or 5 (fine, solid) water molecules at 303 K and for the CG model (thick, solid) at 298 K and 1 atm.

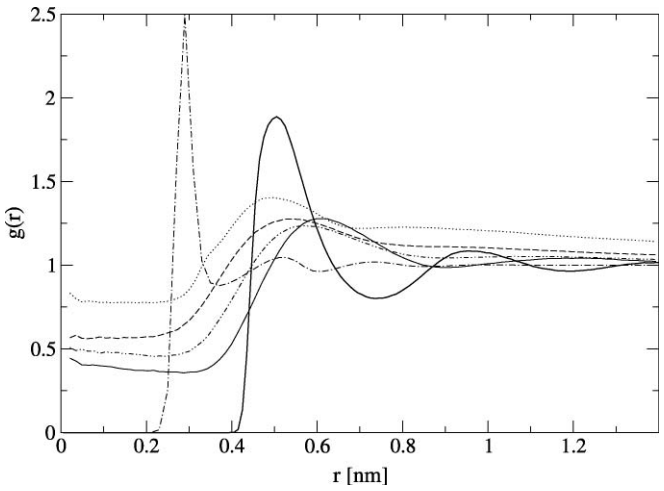

FIG. 5. The radial distribution function (RDF) $g(r)$ [Eq. (8)] in liquid water for the clusters with $n = 1$ (fine, dotted-dashed), 2 (fine, dotted), 3 (fine, dashed), 4 (fine, double-dotted-dashed), or 5 (fine, solid) water molecules and for the CG model (thick, solid), where r is the distance between the centers of geometry (COG) of two clusters or the CW sites of two CG beads, respectively, at 303 K and 1 atm. For clusters with $n = 2$–5, simulations with distance restraining between the molecules of a cluster were used.

cluster decreases with increasing cluster size and the distribution becomes more gaussian-like, indicating a more or less spherical shape for a cluster of five water molecules. The average dipole moments are listed in Table II.

2. Distance restrained simulations

Radial distribution function. In principle, the normalized radial distribution function $g(r)$ should be zero for distances shorter than the first solvation shell, and should converged to 1 for large $r_{\alpha\beta}$. For SPC clusters held together by distance restraints, the center of geometry of two clusters can lie closer together than they ideally would. Therefore for clusters with $n > 1$, the normalization was incomplete as can be seen in Fig. 5. Nevertheless, the $g(r)$ gives a first estimate of the size of a cluster and the minimum distance between two clusters, respectively. The increase in this intercluster distance is largest between small n and levels off with increasing cluster size. For $n = 5$, this distance lies around 0.6 nm.

Self-diffusion coefficient. A simulation time of 1 ns is in general not sufficient to get converged values for the diffusion coefficient D, but as the averaging was also done over different clusters, good statistics could be obtained. The experimental diffusion coefficient D_{exp} for water is 2.3×10^{-5} cm^2 s^{-1}. For SPC water, $D_{n=1} = 5.1 \times 10^{-5}$ cm^2 s^{-1} is found. With increasing cluster size, the diffusion coefficient is decreasing from $D_{n=2} = 2.3 \times 10^{-5}$ cm^2 s^{-1} to $D_{n=5} = 0.93 \times 10^{-5}$ cm^2 s^{-1}. This decrease in diffusion with n can be explained by the fact that the individual water molecules in a cluster may be pulled into different directions resulting in a small net displacement of their center of geometry.

Thermodynamic cycle. Thermodynamic properties like the solvation free energy ΔF_{solv} of a single water molecule can be easily calculated and compared with the experimental value for liquid water. But, for a cluster of water molecules this is not as easy. Clearly, a CG bead representing a number of water molecules larger than one, should not reproduce the experimental value for a single water molecule. Therefore, knowing the thermodynamic behavior of a water cluster is essential for the sake of comparison. To this end, a thermodynamic cycle was simulated using thermodynamic integration,

TABLE III. Density ρ, total potential energy per bead V_{pot}, surface tension γ [Eq. (15)], self-diffusion coefficient D [Eq. (11)], relative static dielectric permittivity $\epsilon(0)$ [Eq. (19)], and shear viscosity η [Eq. (16)] at 298 K of the CG water model in comparison with experimental data and SPC and SPC/E water, as well as with the polarizable MARTINI model and the BMW model. Note that $\epsilon(0)$ of the polarizable MARTINI model, which uses $\epsilon_{cs} = 2.5$, was calculated using the dipole moment fluctuation methodology (Ref. 38) formulated for the case of $\epsilon_{cs} = 1$. $\epsilon(0)$ of the BMW model was obtained from the potential mean force (PMF) between charged ions.

	ρ (g cm^{-3})	V_{pot} (kJ mol^{-1})	γ (mN m^{-1})	D (10^{-5} cm^2 s^{-1})	$\epsilon(0)$	η (cP)
Experiment (Refs. 27 and 33)	0.997	–41.5	71.6	2.3	78.4	0.85
SPC (Refs. 39 and 40)	0.972	–41.3	53.4	4.2	66.6	0.49
SPC/E (Ref. 40)	0.994	...	...	2.4	73.5	0.91
GROMOS CG model	0.995	–23.3	51.2	6.9	73.7	3.72
Pol. MARTINI model (Ref. 20)	1.043	...	30.5	0.625	75.6	...
BMW model (Ref. 19)	1.047	...	77	...	74	...

TABLE IV. Isothermal compressibility κ_T [Eq. (15)] at 298 K of the CG water model in comparison with experimental data and SPC and SPC/E water, as well as for the BMW model. For the polarizable MARTINI CG model no data on the compressibility were reported.

	ρ (g cm^{-3})	p (atm)	κ_T (10^{-5} atm^{-1})
Expt. (Ref. 27)	0.997	1	4.58
SPC (Ref. 39)	0.947	–447.1	
			5.5
	0.997	475.8	
			4.0
	1.047	1706.4	
SPC/E (Ref. 40)	0.994	...	5.2
GROMOS CG model	0.947	–384.9	
			13.8
	0.997	22.6	
			8.4
	1.047	608.3	
BMW model (Ref. 19)	1.047	...	3.3

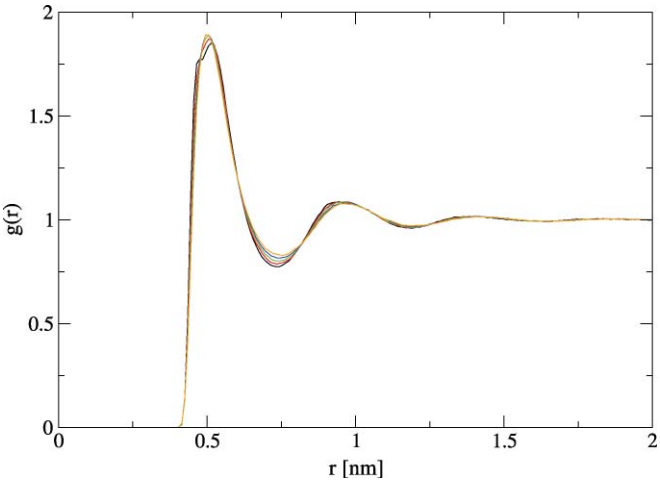

FIG. 6. The radial distribution function (RDF) $g(r)$ [Eq. (8)] from liquid phase simulations with the CG model at different temperatures $T = 258$ (black), 278 (red), 298 (green), 318 (blue) and 338 K (orange) and 1 atm. Here r is the CW–CW distance.

in which the overall free energy difference ΔF_{cycle} should be zero (Fig. 2). The free energy of desolvation $\Delta F_{\text{SPC}}^{\text{liquid}\rightarrow\text{gas}}$ of a single SPC molecule with distance restraints to four dummy water molecules under NVT conditions at 303 K is 28 kJ mol^{-1}. Without distance restraints at 300 K, it is 23 kJ mol^{-1}.[41] For a cluster of five water molecules, a value of 80 kJ mol^{-1} was obtained for the same perturbation. $\Delta F_{\text{Cluster}\rightarrow\text{SPC}}^{\text{liquid}}$ was found to be 106 kJ mol^{-1}, and the analog in the gas phase 55 kJ mol^{-1}. This results in an error of 1 kJ mol^{-1} for the cycle free energy difference ΔF_{cycle}.

B. Coarse-grained simulations

1. Radial distribution function, self-diffusion coefficient and viscosity

The radial distribution function of the CG model in comparison with the SPC clusters is shown in Fig. 5. The peak of the first solvation shell is at a shorter distance than for clusters with $n = 5$, i.e., 0.5 nm instead of 0.6 nm. The CG model was parametrized to reproduce the experimental density at 298 K $\rho = 997$ kg m^{-3}, while the density of SPC water is $\rho = 972$ kg m^{-3}. This too low density results in a too large *inter*cluster distance for SPC water. Due to the explicit electrostatic interactions, the RDF of the CG model is much less structured as normally found for Lennard-Jones liquids. For the CG model, a diffusion coefficient D of 6.9×10^{-5} cm^2 s^{-1} was found, about seven times the value for a cluster of five SPC water molecules. For the shear viscosity η, a value of 3.72 cP (centipoise) was obtained which is larger than the measured viscosity of water. This reflects a reduced momentum transfer in the CG model.

2. Dipole moment and dielectric permittivity

The dipole moment distribution obtained with the CG model compared with those of the SPC clusters is shown in Fig. 4. The distribution for CG water is narrower than the distribution of the ($n = 5$) cluster, as a single dipole is used to model the cluster dipole consisting of five molecular dipoles. The average dipole moment of 6.4 Debye, however, is very close to the one found for the clusters, 6.1 Debye. The dielectric permittivity $\epsilon(0)$ of 73.7 of the CG model is close to the experimental permittivity of water $\epsilon(0) = 78.4$ (Ref. 33) (Table III). The rotational correlation time τ_{rot} of the dipole moment of the CG beads was calculated and compared with that of a SPC cluster. The decay of both functions is similar with $\tau_{\text{rot}} = 5.6$ ps^{-1} for both the CG model and a SPC cluster.

Thermodynamic properties. Thermodynamic properties calculated at 298 K are listed in Tables III–V. The surface tension γ is a critical property which should be reproduced, especially when the model is to be used together with lipid membranes. For the CG model, an average surface tension

TABLE V. Thermal expansion coefficient α [Eq. (12)] and the heat capacity C_p [Eq. (13)] at 1 atm pressure of the CG water model in comparison with experimental data and SPC and SPC/E water. For the polarizable MARTINI CG model and the BMW model no data on the thermal expansion coefficient and heat capacity were reported.

	T (K)	ρ (g cm^{-3})	α (10^{-4} K^{-1})	C_p (J mol^{-1} K^{-1})
Experiment (Ref. 27)	298	0.997	2.57	75.32
	318	0.990	4.22	75.31
	338	0.980	5.54	75.43
SPC (Ref. 39)	298	0.972		
			8.1	64.2
	318	0.956		
			10.0	73.7
	338	0.937		
SPC/E (Ref. 40)	298	0.994	5.6	80.1
GROMOS CG model	298	0.995		
			23	80.7
	318	0.951		
			26	85.7
	338	0.901		

γ of 51.2 ± 1.8 mN m^{-1} was found which is similar to the value of 53.4 mN m^{-1} for SPC water. For the isothermal compressibility κ_T, values of 13.8×10^{-5} and 8.4×10^{-5} atm^{-1} were obtained, which are higher than in experiment. Thermal expansion coefficients α of 2.3×10^{-3} and 2.6×10^{-3} K^{-1} were found. These values are much higher than in experiment which is to be expected due to the larger Lennard-Jones radii of the CG beads. The softer Lennard-Jones interaction between CG beads is reflected in the higher heat capacity of 80.7 and 85.7 J mol^{-1} K^{-1} obtained for the CG model compared with 75.3 J mol^{-1} K^{-1} measured for water. The excess free energy of the CG beads was calculated using TI simulations. The perturbation was performed for all particles and the resulting free energy difference was divided by the number of beads, giving $\Delta F_{\mathrm{CG}}^{\mathrm{liquid}\rightarrow\mathrm{gas}} = 11.1$ kJ mol^{-1} per CG bead. The remaining potential energy in the gas phase due to the unconstrained bond is 0.4 kJ mol^{-1} per bead, thus $\Delta U_{\mathrm{CG}}^{\mathrm{liquid}\rightarrow\mathrm{gas}} = 22.9$ kJ mol^{-1} per bead.

3. Temperature range

The temperature-dependent behavior of the CG model was investigated by performing simulations at different temperatures ranging from 258 to 338 K under NpT conditions. As can be seen in Fig. 6, the $g(r)$ becomes more structured with decreasing temperature. At 258 K, first signs of freezing can be observed as a splitting in the first peak.

4. Variation of model parameters

Based on separate simulations and the observations made during the parametrization process, the effects of the variation of single model parameters on the properties of the CG model are summarized in Table VI. The impact of the various parameters on the density, the potential energy per bead, and the self-diffusion coefficient is easily understandable. The effect on the surface tension, the average dipole moment per bead, and the relative static dielectric permittivity appears to be more complex in certain cases. A decrease in the potential energy per bead correlates with an increase in the density of the system and a decrease of the diffusion coefficient. A decrease in the potential energy results, however, not in all cases in a higher surface tension, and a higher average dipole moment leads not necessarily to a higher dielectric permittivity. When increasing C_{12}, the Lennard-Jones interaction is more repulsive and thus the potential energy per bead becomes more positive resulting in a lower density, surface tension and dielectric permittivity, as well as a higher diffusion coefficient while the average dipole moment remains unchanged. An increase in C_6 on the other hand leads to a lower potential energy, thus a higher density, dielectric permittivity and surface tension, as well as a lower diffusion coefficient while the average dipole moment remains again unchanged. Changing the ratio between the masses of the central and the dipole particle only affects the diffusion coefficient. Two effects interact here. If the two particles have similar masses, they can move with similar inertia in opposite directions resulting in a small net displacement. On the other hand, a large mass slows a particle down. If the two particles have the same mass, 45 amu, the first effect is largest. If the central particle is much heavier than the dipole particle, e.g., a ratio of 80:10, the motion of the central particle is slowed down, but the dipole particle cannot pull in another direction thus the displacement depends only on the central particle. The smallest diffusion coefficient is therefore found for a mass ratio of 0.5. If K_b becomes larger, the oscillation of the dipole particle is more restricted resulting in a lower average dipole moment and thus a higher potential energy per bead and diffusion coefficient, a lower density, dielectric permittivity, and surface tension. In-

TABLE VI. Effect of a variation of CG model parameters on the liquid state properties of the CG model if taken independently. The trends represented are based on separate simulations and the observations made during the process of parametrization. Parentheses indicate a weak effect.

	ρ	V_{pot}	γ	D	$\epsilon(0)$	$\langle\mu\rangle$
Increase C_{12}	↓	↑	↓	↑	↓	...
Increase C_6	↑	↓	↑	↓	↑	...
Increase $m_{\mathrm{DP}}/m_{\mathrm{CW}}$	...	...	...	↓↑	...	...
Increase K_b	↓	↑	↓	↑	↓	↓
Increase q	↑	↓	(↑)	↓	↓	↑
Increase $r_{\mathrm{CW-DP}}$	↑	↓	(↑)	↓	↓	↑
Decrease ϵ_{cs}	↑	↓	(↑)	↓	↓	↑

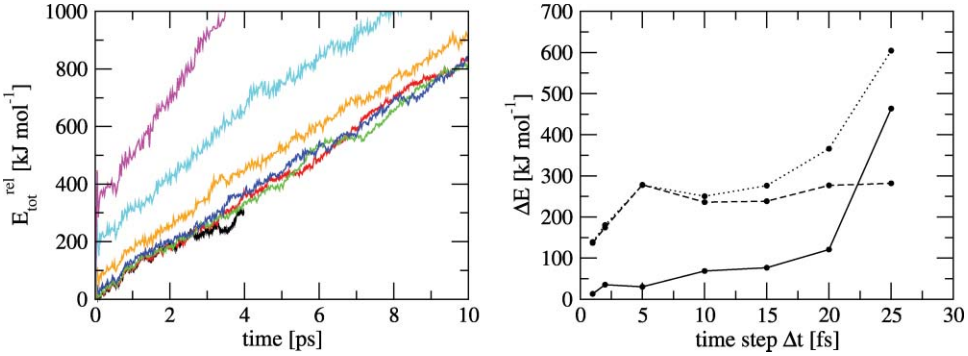

FIG. 7. (Left) Time series of the relative total energy of the system $E_{\mathrm{tot}}^{\mathrm{rel}}(t) = E_{\mathrm{tot}}(t) - E_{\mathrm{tot}}(0)$ for different time steps $\Delta t = 2$ (black), 5 (red), 10 (green), 15 (blue), 20 (orange), 25 (cyan), and 28 fs (magenta). The simulations were performed for a system of 2560 CG beads for 2000 steps under NVE conditions at 298 K. The nonbonded cut-off was 2.0 nm and the pairlist was updated every step. (Right) Fluctuations of the total energy ΔE_{tot} (solid) compared to those of the kinetic ΔE_{kin} (dashed) and the potential energy ΔE_{pot} (dotted line) as a function of the integrations time step. Simulations were performed for 5000 steps under NVE conditions at 298 K. The nonbonded cut-off was set to 3.5 nm and the pairlist was updated every step.

creasing the partial charges of the two particles in a bead or the ideal bond length, or decreasing the dielectric permittivity inside the cut-off sphere result in a higher average dipole moment, but not a higher dielectric permittivity together with a lower potential energy and diffusion coefficient, and a higher density, while the surface tension increases only slightly.

Integration time step and speed-up. There exist a number of sources or sinks of heat in MD simulations: nonconservative forces, the use of constraints, temperature, and pressure coupling, the nonbonded interaction cut-off and the integration time step. In simple NVE simulations without constraints or with a very low tolerance of 10^{-8} for the SHAKE algorithm, only the latter two sources remain. For a sufficiently small time step at a given nonbonded cut-off, the cut-off noise is dominating the total energy fluctuation. For fine-grained molecular models, the error in the nonbonded energy Lennard-Jones term is below 1% at a cut-off of 1.4 nm.[42] For this cut-off, a time step of 2 fs was found to be sufficiently small. The same time step was used conservatively in all CG simulations presented here, leading to a speed-up in computer time of a factor 9 for the same amount of water molecules, i.e., 12 800 SPC molecules versus 2560 CG beads. Due to the large size of the CG beads and the larger cut-off used, a larger time step may be chosen which would increase the speed-up even further. A series of NVE simulations with different time steps was performed to evaluate the largest usable time step for a non-bonded cut-off of 2.0 nm while conserving the total energy of the system. In Fig. 7(a), the time evolution of the relative total energy $E_{\text{tot}}^{\text{rel}}(t) = E_{\text{tot}}(t) - E_{\text{tot}}(0)$ for different time steps Δt is shown. For $\Delta t < 20$ fs, the slope of the total energy is similar for the different time steps, indicating that the dominating heat source is the nonbonded cut-off. For $\Delta t \geq 20$ fs, however, the slope increases with Δt. Additional NVE simulations at a larger cut-off of 3.5 nm were performed to confirm the findings. At a large enough cut-off and a small enough time step, the average fluctuation $\Delta E = \langle (E - \langle E \rangle)^2 \rangle^{1/2}$ of the total energy E_{tot} must be much smaller than the average fluctuation of the kinetic energy E_{kin}.[17] As can be seen in Fig. 7(b), ΔE_{tot} starts to increase significantly after a time step of 15 fs and becomes larger than ΔE_{kin} between 20 and 25 fs. Thus, a maximum integration time step of maximum 15 fs could be used in a simulation with the CG model, which corresponds to an overall speed-up of a factor 70 compared with an all-atom simulation using $\Delta t = 2$ fs and $R_c = 1.4$ nm.

IV. SUMMARY AND CONCLUSIONS

In this study, a polarizable model for coarse-grained water was presented, which treats the electrostatics explicitly by simulating a dipole. The model maps five water molecules into a coarse-grained bead with two oppositely charged interaction sites. The parameters were fitted to reproduce the experimental density and relative static dielectric permittivity of water at 298 K while maintaining the liquid phase. Various structural and thermodynamic properties were calculated and compared with measured ones, with those of SPC water, and if available to those with other CG models. The thermal expansion coefficient of the CG model was an order of magnitude too large compared with the experiment, which is expected due to the larger Lennard-Jones radius of the CG beads compared with that of oxygen. The isothermal compressibility was found to be closer but still larger than the experimental value due to softer interactions between the CG beads compared to molecular water. The surface tension obtained for the CG model is similar to the surface tension of SPC water. These findings show clearly that some properties of the liquid phase can no longer be reproduced when going from the atomistic level to a coarse-grained level. The CG model proposed offers a speed-up of a factor 9 through the reduction of the number of interaction sites for a time step of 2 fs as used in fine-grained simulations. In addition, the time step can be increased up to 15 fs while conserving the total energy of the system, resulting in a total speed-up of a factor 70. Although this CG water cannot form hydrogen bonds, it is polarizable and has the correct relative static dielectric permittivity to describe the electrostatic effects of water. In a next step, the solvation of fine-grained particles in CG water will be investigated.

ACKNOWLEDGMENTS

We thank Philippe Hünenberger for useful discussions. This work was financially supported by the National Center of Competence in Research (NCCR) in Structural Biology and by Grant No. 200020-121913 of the Swiss National Science Foundation, and by Grant No. 228076 of the European Research Council, which is gratefully acknowledged.

[1] Y. Liu and T. Ichiye, J. Phys. Chem. **100**, 2723 (1996).
[2] E. A. Jagla, J. Chem. Phys. **111**, 8980 (1999).
[3] S. Garde and H. S. Ashbaugh, J. Chem. Phys. **115**, 977 (2001).
[4] J. C. Shelley, M. Y. Shelley, R. C. Reeder, S. Bandyopadhyay, and M. L. Klein, J. Phys. Chem. B **105**, 4464 (2001).
[5] S. J. Marrink, A. H. de Vries, and A. E. Mark, J. Phys. Chem. B **108**, 750 (2004).
[6] V. Molinero and W. A. Goddard, J. Phys. Chem. B **108**, 1414 (2004).
[7] S. Izvekov and G. A. Voth, J. Chem. Phys. **123**, 134105 (2005).
[8] M. Praprotnik, S. Matysiak, L. Delle Site, K. Kremer, and C. Clementi, J. Phys.: Condens. Matter **19**, 292201 (2007).
[9] W. Shinoda, R. Devane, and M. L. Klein, Mol. Simul. **33**, 27 (2007).
[10] H. Wang, C. Junghans, and K. Kremer, Eur. Phys. J. E **28**, 221 (2009).
[11] M. E. Johnson, T. Head-Gordon, and A. A. Louis, J. Chem. Phys. **126**, 144509 (2007).
[12] P. Kowalczyk, P. A. Gauden, and A. Ciach, J. Phys. Chem. B **113**, 12988 (2009).
[13] X. He, W. Shinoda, R. DeVane, and M. L. Klein, Mol. Phys. **108**, 2007 (2010).
[14] K. R. Hadley and C. McCabe, J. Phys. Chem. B **114**, 4590 (2010).
[15] A. P. Lyubartsev and A. Laaksonen, Phys. Rev. E **52**, 3730 (1995).
[16] D. Reith, M. Puetz, and F. Mueller-Plathe, J. Comput. Chem. **24**, 1624 (2003).
[17] M. Winger, D. Trzesniak, R. Baron, and W. F. van Gunsteren, Phys. Chem. Chem. Phys. **11**, 1934 (2009).
[18] T. Ha-Duong, N. Basdevant, and D. Borgis, Chem. Phys. Lett. **468**, 79 (2009).
[19] Z. Wu, Q. Cui, and A. Yethiraj, J. Phys. Chem. B **114**, 10524 (2010).
[20] S. O. Yesylevskyy, L. V. Schäfer, D. Sengupta, and S. J. Marrink, PLOS Comput. Biol. **6**, e1000810 (2010).
[21] C. Oostenbrink, A. Villa, A. E. Mark, and W. F. van Gunsteren, J. Comput. Chem. **25**, 1656 (2004).
[22] H. J. C. Berendsen, J. P. M. Postma, W. F. van Gunsteren, and J. Hermans, in *Intermolecular Forces*, edited by B. Pullmann (Reidel, Dordrecht, 1981), pp. 331–342.

[23]M. Christen, P. H. Hünenberger, D. Bakowies, R. Baron, R. Bürgi, D. P. Geerke, T. N. Heinz, M. A. Kastenholz, V. Kräutler, C. Oostenbrink, C. Peter, D. Trzesniak, and W. F. van Gunsteren, J. Comput. Chem. **26**, 1719 (2005).
[24]H. J. C. Berendsen, J. R. Grigeraand, and T. P. Straatsma, J. Phys. Chem. **91**, 6269 (1987).
[25]W. F. van Gunsteren, R. Boelens, R. Kaptein, R. M. Scheek, E. R. P. Zuiderweg, in *Molecular Dynamics and Protein Structure*, edited by J. Hermans (Polycrystal Book Services, Western Springs, 1985), pp. 5–14.
[26]S. Riniker, A. -P. E. Kunz, and W. F. van Gunsteren, On the calculation of the dielectric permittivity of molecular models in the liquid phase, J. Chem. Theory Comput. (submitted).
[27]A. P. Kunz and W. F. van Gunsteren, J. Phys. Chem. A **113**, 11570 (2009).
[28]H. J. C. Berendsen, J. P. M. Postma, W. F. van Gunsteren, A. DiNola, and J. R. Haak, J. Chem. Phys. **81**, 1517 (1984).
[29]I. G. Tironi, R. Sperb, P. E. Smith, and W. F. van Gunsteren, J. Chem. Phys. **102**, 5451 (1995).
[30]T. N. Heinz, W. F. van Gunsteren, and P. H. Hünenberger, J. Chem. Phys. **115**, 1125 (2001).
[31]J.-P. Ryckaert, G. Ciccotti, and H. J. C. Berendsen, J. Comput. Phys. **23**, 327 (1977).
[32]T. B. Beutler, A. E. Mark, R. C. van Schaik, P. R. Gerber, and W. F. van Gunsteren, Chem. Phys. Lett. **222**, 529 (1994).
[33]D. R. Lide, *Handbook of Chemistry and Physics*, 88th ed. (CRC/Taylor and Francis, Boca Raton, FL, 2007–2008).
[34]H. J. C. Berendsen, *Simulating the Physical World*, 1st ed. (Cambridge University Press, Cambridge, 2007).
[35]I. G. Tironi and W. F. van Gunsteren, Mol. Phys. **83**, 381 (1994).
[36]B. J. Berne and R. Pecore, *Dynamic Light Scattering with Applications to Chemistry, Biology, and Physics* (Wiley, New York, 1976).
[37]K. A. Motakabbir and M. Berkowitz, J. Phys. Chem. **94**, 8359 (1990).
[38]M. Neumann, Mol. Phys. **50**, 841 (1983).
[39]H. B. Yu, T. Hansson, and W. F. van Gunsteren, J. Chem. Phys. **118**, 221 (2003).
[40]A. Glättli, X. Daura, and W. F. van Gunsteren, J. Chem. Phys. **116**, 9811 (2002).
[41]C. Peter, C. Oostenbrink, A. van Dorp, and W. F. van Gunsteren, J. Chem. Phys. **120**, 2652 (2004).
[42]X. Daura, A. E. Mark, and W. F. van Gunsteren, J. Comput. Chem. **19**, 535 (1998).